Acta Cryst A FOUNDATIONS ADVANCES

ISSN 2053-2733

Structure refinement using precession electron diffraction tomography and dynamical diffraction: theory and implementation

Lukáš Palatinus,[a]* Václav Petříček[a] and Cinthia Antunes Corrêa[a,b]

[a]Institute of Physics of the AS CR, Na Slovance 2, Prague, Czech Republic, and [b]Department of Physics of Materials, Charles University, Prague 12116, Czech Republic. *Correspondence e-mail: palat@fzu.cz

Received 20 November 2014
Accepted 21 January 2015

Keywords: dynamical diffraction; electron diffraction tomography; electron crystallography.

Accurate structure refinement from electron-diffraction data is not possible without taking the dynamical-diffraction effects into account. A complete three-dimensional model of the structure can be obtained only from a sufficiently complete three-dimensional data set. In this work a method is presented for crystal structure refinement from the data obtained by electron diffraction tomography, possibly combined with precession electron diffraction. The principle of the method is identical to that used in X-ray crystallography: data are collected in a series of small tilt steps around a rotation axis, then intensities are integrated and the structure is optimized by least-squares refinement against the integrated intensities. In the dynamical theory of diffraction, the reflection intensities exhibit a complicated relationship to the orientation and thickness of the crystal as well as to structure factors of other reflections. This complication requires the introduction of several special parameters in the procedure. The method was implemented in the freely available crystallographic computing system *Jana2006*.

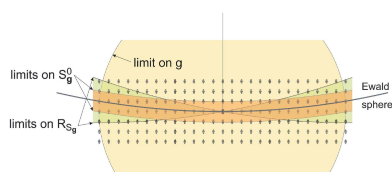

© 2015 International Union of Crystallography

1. Introduction

Structure solution and refinement from single-crystal X-ray diffraction data has become a standard approach for determination of crystal structures. On the other hand, electron diffraction used to be applied for the same purpose much more rarely, although numerous successful solutions were reported (Vainshtein, 1964; Cowley, 1992; Dorset, 1995). The situation has been changing rapidly in the past decade with the advent of electron diffraction tomography (EDT) methods (Kolb *et al.*, 2007, 2008; Wan *et al.*, 2013), possibly combined with precession electron diffraction (PED) (Vincent & Midgley, 1994; Mugnaioli *et al.*, 2009). With these methods, a large number of increasingly complex structures were solved and refined. However, all the structure refinements were performed using kinematical approximation for the calculation of model intensities. Kinematical approximation implies that diffracted intensity associated with diffraction vector $\mathbf{h}$ is proportional to the amplitude squared of the corresponding structure factor $F_{\mathbf{h}}$. It is, however, well known that this approximation has only limited validity for electron-diffraction data. Measures have been taken to minimize the departure of the electron-diffraction data from the kinematical limit by integrating the diffracted intensities across several beam orientations (using precession electron diffraction or fine-step slicing in rotation electron diffraction). Despite these measures, the refinements using this approximation are difficult, and yield high figures of merit and low accuracy of the refined structure parameters.

An obvious remedy to this problem is avoiding the kinematical approximation in the calculation of diffracted intensities, and instead using the correct dynamical-diffraction theory. This approach has indeed been taken in the past (Jansen *et al.*, 1998; Dudka *et al.*, 2008; Oleynikov, 2011). However, it has always been performed on oriented diffraction patterns, while for a robust and complete structure refinement it is necessary to refine the structure against a three-dimensional data set, and ideally maintain a high data-to-parameter ratio. Such data are obtained with electron diffraction tomography techniques. We have therefore decided to develop and implement a structure refinement technique that would use a series of non-oriented electron-diffraction patterns obtained by EDT, and calculated model intensities using full dynamical calculations. The first steps towards this goal were described in a previous paper [Palatinus *et al.* (2013), denoted paper I hereafter]. In paper I we have used oriented diffraction patterns of three compounds to show that using dynamical diffraction indeed yields results superior to the kinematical approximation. Moreover, we have also shown that using PED provides results with better figures of merit, stable refinements and more accurate structure parameters. The method presented in this work can be applied to data collected by EDT with, as well as without, precession.

2. Theory

2.1. Dynamical diffraction – calculation of diffracted intensities

The theory of electron diffraction by crystals is well elaborated and several excellent sources with various degrees of detail and complexity are available. In this work we used the Bloch-wave formalism for the calculation of diffracted intensities. We outline only the basic formulae used in the calculation. The formulation used in this section is based on the book *Electron Microdiffraction* by Spence & Zuo (1992). Another useful source of information is the book *Electron Microscopy of Thin Crystals* by Hirsch *et al.* (1977) or the excellent treatise by Metherel (1975).

When back-scattering of electrons is ignored, the diffraction can be described by means of a scattering matrix **S**, which relates the diffracted waves at thickness t [$\varphi_{\mathbf{g}}(t)$] with the incident waves on the crystal surface [$\varphi_{\mathbf{g}}(0)$]. The scattering matrix is obtained by exponentiation of the so-called structure matrix **A**:

$$\mathbf{S} = \mathbf{M}\exp\left(\frac{2\pi i t}{2K_n}\mathbf{A}\right)\mathbf{M}^{-1}. \quad (1)$$

This formula can be rewritten explicitly using the eigenvector matrix **B** and diagonal eigenvalue matrix $\boldsymbol{\Lambda}$ of the structure matrix **A**:

$$\mathbf{S} = \mathbf{MB}\exp\left(\frac{2\pi i t}{2K_n}\boldsymbol{\Lambda}\right)\mathbf{B}^{-1}\mathbf{M}^{-1}. \quad (2)$$

The following quantities enter this expression directly or indirectly:

(*a*) t: the thickness of the crystal slab.

(*b*) $\{\mathbf{g}_i, i = 1\ldots n\}$: a set of n diffraction vectors of excited beams considered in the calculation.

(*c*) **n**: normal to the entrance surface of the crystal pointing out from the crystal towards the source of electrons.

(*d*) **K**: wavevector of the incident beam with amplitude corrected for the mean inner potential U_0 of the crystal. $|K| = (K_0^2 + U_0)^{1/2}$, with K_0 being the wavevector amplitude in vacuum.

(*e*) g_n, K_n: the projections of the vectors **g** and **K** onto the surface normal **n**. $g_n = \mathbf{g}\cdot\mathbf{n}$, $K_n = \mathbf{K}\cdot\mathbf{n}$.

(*f*) Structure matrix **A**: a square matrix with number of rows equal to the number of excited beams considered in the calculation. The diagonal elements of **A** are given by

$$a_{ii} = \frac{|\mathbf{K}|^2 - |\mathbf{K}+\mathbf{g}_i|^2}{(1+g_{n,i}/K_n)^{1/2}}. \quad (3)$$

The off-diagonal elements are

$$a_{ij} = \frac{U_{\mathbf{g}_i-\mathbf{g}_j}}{(1+g_{n,i}/K_n)^{1/2}(1+g_{n,j}/K_n)^{1/2}}. \quad (4)$$

(*g*) **M**: a diagonal matrix with elements

$$m_{ii} = 1/(1+g_{n,i}/K_n)^{1/2}. \quad (5)$$

Note that the formulae simplify considerably if only beams with **g** parallel to the crystal surface are excited. In such case $g_{n,i} = 0$ and matrix **M** is an identity matrix. This assumption is frequently used to calculate zero-order Laue-zone diffraction from an oriented crystal slab. This condition, however, is almost never fulfilled for EDT data, and full calculation including the non-zero g_n term should be used.[1]

If the incident wavefield consists of only one incident beam, the diffracted waves at thickness t are given by the elements of the first column of the scattering matrix, and the diffracted intensities are obtained as the amplitude squared of these elements:

$$I_{\mathbf{g}_i} = |s_{i1}|^2. \quad (6)$$

These expressions allow calculation of diffracted intensities in the general case of a non-oriented diffraction pattern taken on a tilted crystal. Absorption effects can be included through additional imaginary terms in the structure factors $U_{\mathbf{g}}$ (Bird & King, 1990; Weickenmeier & Kohl, 1991). The most important limitation of this procedure is the assumption that the crystal is a slab of constant thickness.

For practical calculation it is convenient to select a Cartesian coordinate system such that the x axis lies in the rotation axis of the goniometer, the z axis points towards the beam and the y axis completes the right-handed system. Then the wavevector of the incident beam in this Cartesian system is

[1] Note that the formulae presented in paper I do not include this effect and are thus valid exactly only for oriented patterns with zone axis parallel to the crystal surface normal.

$\mathbf{K} = (0, 0, -|\mathbf{K}|)$, and the vector $\mathbf{g}$ with indices (h, k, l) expressed in the crystal's reciprocal space can be transformed into the coordinates (x, y, z) of the Cartesian system by means of the orientation matrix **UB**. According to the standard definition, the *i*th column of **UB** contains the Cartesian coordinates of the coordinates of the *i*th basic vector of the reciprocal lattice, and the transformation is thus $(x, y, z)^{\mathrm{T}} = \mathbf{UB} \cdot (h, k, l)^{\mathrm{T}}$.

Structure refinement by the least-squares method requires knowledge of the derivatives of the intensities with respect to structure parameters. These derivatives can always be estimated using the method of finite differences. However, explicit formulae exist that are significantly faster than numerical evaluation of the derivatives. In this work we used the formulation described *e.g.* in van der Aa *et al.* (2007), where explicit formulae for the derivatives of the eigenvector matrix $\mathbf{B}$ and eigenvalue matrix $\boldsymbol{\Lambda}$ are derived, if the derivative of the structure matrix $\mathbf{A}$ is known. The off-diagonal elements of the matrix $\mathbf{A}$ are the structure factors, and their derivatives with respect to the structure parameters are thus readily available. Once the derivatives $\mathrm{d}\mathbf{B}/\mathrm{d}p$ and $\mathrm{d}\boldsymbol{\Lambda}/\mathrm{d}p$ are known, the intensity derivatives $\mathrm{d}I_{\mathbf{h}}/\mathrm{d}p$ can be calculated with only two matrix–matrix multiplications and a small number of matrix–vector multiplications, making the procedure several times faster than two matrix diagonalizations necessary for the calculation of the derivatives using the method of central finite differences.

2.2. Using precession electron diffraction with dynamical calculations

Precession electron diffraction is generally regarded as a technique that suppresses the dynamical character of diffracted intensities (Vincent & Midgley, 1994; Berg *et al.*, 1998; Mugnaioli *et al.*, 2009). The intensities obtained with PED tend to be closer to the kinematical limit than intensities obtained without precession. It might thus appear superfluous to use precession electron diffraction, if dynamical-diffraction theory is used. However, it was shown in Own *et al.* (2006) and in detail in paper I that this combination is very useful. The PED intensities are much less sensitive to crystal imperfections like thickness variations or slight bending, and more sensitive to the variation of structural parameters. Hence, diffraction data obtained with PED can be fitted more accurately than non-PED data and they yield more accurate structural parameters. The price to pay for this improvement is the increased computing time. PED intensities are an integral over all orientations of the primary beam along the precession circuit, and calculation of the intensities requires evaluation of the dynamical-diffraction pattern in a number of beam orientations. It was shown in paper I (see Fig. 5 therein) that the necessary number of integration steps may range from 100 to over 500 depending on the sample thickness.

2.3. Data processing and intensity extraction

The data processing for dynamical refinement from EDT data is very similar to the procedure described for EDT data previously (Kolb *et al.*, 2007, 2008; Palatinus *et al.*, 2011). It involves the following steps:

(i) Peak hunting: locating positions of reflections on each diffraction pattern.

(ii) Indexing: determining the unit-cell parameters and orientation matrix from the reflection positions.

(iii) Integration: determination of integrated intensities for each reflection.

Data processing for dynamical refinement is specific in the integration step. It is obvious from §2.1, equation (3), that the dynamical intensities depend on the orientation of the crystal (through the term $|\mathbf{K}+\mathbf{g}|^2$), and the intensity of the same reflection on subsequent frames is not a simple function of the crystal orientation, as in the kinematical case. The dependence is even more complicated for PED data. It is therefore necessary to fit intensities on each pattern separately. The input for the dynamical refinement is thus the orientation matrix of the crystal, a list of positional angles for each recorded diffraction pattern, and then a list of reflection indices, intensities and e.s.d.'s of the intensities together with the identifier of the pattern on which the reflection was recorded. If the same reflection appears on more consecutive patterns, it may appear in the list several times, once for every pattern on which it was recorded.

A reflection is included in the output list if it is for a given pattern close enough to the exact Bragg condition. The deviation of the reflection from exact Bragg condition can be measured by excitation error $S_{\mathbf{g}}$. $S_{\mathbf{g}}$ is the distance of the reciprocal-lattice node from the Ewald sphere. $S_{\mathbf{g}}$ can be calculated to a good approximation as

$$S_{\mathbf{g}} \simeq \frac{|\mathbf{K}|^2 - |\mathbf{K}+\mathbf{g}|^2}{2|\mathbf{K}|}. \qquad (7)$$

All reflections with $S_{\mathbf{g}}$ smaller than a certain threshold $S_{\mathbf{g}}^{\mathrm{int}}$ should be considered present on a given frame and their intensities should be determined. $S_{\mathbf{g}}^{\mathrm{int}}$ is the only parameter of the integration procedure specific to the data processing for dynamical refinement.

2.4. Data selection

Each recorded pattern is populated with a certain set of reflections, and each of these reflections can be characterized by a number of quantities. The most important for the refinement are the following:

(*a*) The length of the diffraction vector $\mathbf{g}$.

(*b*) Excitation error of the reflection without taking the precession into account $S_{\mathbf{g}}^{0}$: this excitation error can be calculated from equation (7).

(*c*) Minimum and maximum excitation error reached during the precession circuit $S_{\mathbf{g}}^{\min}$ and $S_{\mathbf{g}}^{\max}$: it follows directly from the geometry of the PED that the minimum and maximum excitation errors for reflection $\mathbf{g}$ are given by the following formulae (valid for small angles φ):

$$S_{\mathbf{g}}^{\min} \simeq S_{\mathbf{g}}^{0} - |\mathbf{g}|\varphi, \qquad (8)$$

$$S_{\mathbf{g}}^{\max} \simeq S_{\mathbf{g}}^{0} + |\mathbf{g}|\varphi. \quad (9)$$

(*d*) The ratio $R_{S_{\mathbf{g}}} = |S_{\mathbf{g}}^{0}|/(|\mathbf{g}|\varphi)$: this ratio expresses how well the reflection is 'covered' by the precession motion. If $R_{S_{\mathbf{g}}} < 1$, then the reflection passes through the exact Bragg condition twice during the precession circuit. For $R_{S_{\mathbf{g}}} = 1$ the precession motion reaches the Bragg condition at one point, and for $R_{S_{\mathbf{g}}} > 1$ the reflection never reaches the exact Bragg condition. Note that $R_{S_{\mathbf{g}}} > 1$ does not necessarily imply the reflection is weak or absent. A strong reflection may give appreciable signal even relatively far away from the exact Bragg condition, especially for very thin samples.

When processing a diffraction pattern, the program must decide which reflections will be treated as experimentally observed on the pattern. Each of the quantities outlined above can be used for this purpose. The limitation on the length of **g** has an obvious meaning of deciding on the maximum resolution of the diffraction data. Setting a limit on $S_{\mathbf{g}}^{0}$ is a way of limiting the data set only to the reflections within a certain distance from the Ewald sphere. $R_{S_{\mathbf{g}}}$ is a less obvious, yet very useful filter. Setting a limit on $R_{S_{\mathbf{g}}}$ smaller than 1 results in accepting only reflections that passed through the exact Bragg condition. Such reflections are less affected by crystal imperfections, mosaicity and bending, while reflections with large $R_{S_{\mathbf{g}}}$ are more affected by these effects. This is due to the fact that the primary effect of mosaicity, bending and other crystal imperfections in the reciprocal space can be described as a convolution of the perfect diffraction pattern with a certain smearing function. Integrating the complete or almost complete intensity of the reflection (*i.e.* $R_{S_{\mathbf{g}}}$ significantly smaller than 1) makes the integrated intensity insensitive to the smearing, while if only a small part of the reflection is integrated, the smearing can have a significant effect on the resulting intensity. The filters on $S_{\mathbf{g}}^{0}$ and on $R_{S_{\mathbf{g}}}$ may be combined. Fig. 1 shows graphically the meaning of the data-selection filters.

2.5. Models for thickness variation in the sample

It is extremely difficult to derive exact expressions for diffracted intensities from a crystal with a general irregular shape. Such calculation does not only require exact knowledge of the crystal shape, but also the coherence properties of the electron beam. Moreover, diffraction on a slab with non-parallel surfaces results in splitting of the beam into several branches (Spence & Zuo, 1992; Metherel, 1975), making the whole problem even more complicated. However, in most electron-diffraction experiments no special care is taken to make the beam coherent. If the crystal is not too irregular, then the transversal coherence length can be considered small compared to the variation of the thickness in the crystal. If the angular deviation of the normals to opposite surfaces is also assumed to be small, then the crystal can be approximated by a collection of small, parallel slabs with varying thickness (Figs. 2*a*, 2*b*), and the diffracted intensities can be calculated as an incoherent sum of diffraction patterns emerging from each of these small slabs. In such a case the relative position of these small slabs is not important, and therefore the shape of the crystal need not be known in detail. The only quantity needed for the calculation of the intensities is the probability density distribution of thickness across the crystal. To further simplify the problem, the shape of the crystal may be approximated by some simple geometric shape like a wedge, a lens or a cylinder (Fig. 2*c*), and for these shapes the thickness probability density can be derived analytically. Some of these analytical expressions are derived in Appendix *A*. Because PED intensities exhibit relatively low sensitivity to thickness variation, using these simple geometric approximations to crystal shapes should be a simple, but sufficiently adequate way of describing the thickness variation effects.

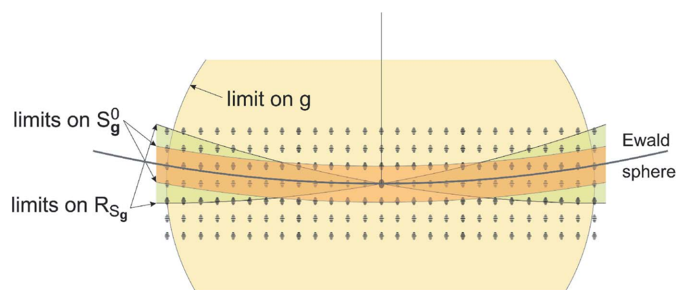

Figure 1
Schematic representation of the Ewald construction with different data-selection criteria shown as filled areas of different colours. Yellow area: reflections passing the limit on the length of **g** (limit on resolution). Orange area: reflections passing the limit on $S_{\mathbf{g}}^{0}$. Green area: reflections passing the limit on $R_{S_{\mathbf{g}}}$.

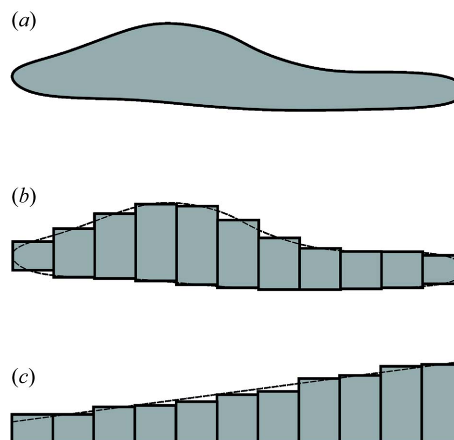

Figure 2
(*a*) Schematic representation of an irregular crystal. (*b*) Approximation of the crystal by a set of small blocks with constant thickness. (*c*) If the blocks from (*b*) are rearranged from thinnest to thickest, another crystal is obtained, which, within the approximation of incoherent addition of diffraction from individual blocks, gives the same diffraction pattern as the crystal in (*b*). The dashed line in (*c*) shows that this crystal, and thus also the original crystal shown in (*a*), can be approximated to a good accuracy by a simple wedge.

2.6. Orientation of the patterns

The orientation of the crystal at the moment of recording the diffraction pattern is a critical quantity for the calculation of the diffracted intensities. The orientation can be deter-

Table 1
New entries introduced in the CIF file produced by *PETS*.

These entries define the frames and they link individual entries of the reflection list to the frame on which they were measured.

Dictionary entry	Data type	Definition
(1) Entries in the category `_diffrn_[]`		
`_diffrn_frame_id`	Integer number	Integer identifier of the frame. Used to assign reflections to a frame by means of the dictionary entry `_refln_frame_id`
`_diffrn_frame_u`	Number	First coordinate of the normal to the frame plane expressed in crystal coordinate system
`_diffrn_frame_v`	Number	Second coordinate of the normal to the frame plane expressed in crystal coordinate system
`_diffrn_frame_w`	Number	Third coordinate of the normal to the frame plane expressed in crystal coordinate system
`_diffrn_frame_precession_angle`	Number	Precession angle used for the frame (in degrees)
`_diffrn_frame_alpha`	Number	Rotation of the crystal from the zero position of the goniometer around the principal goniometer axis (in degrees)
`_diffrn_frame_beta`	Number	Rotation of the crystal from the zero position of the goniometer around the axis perpendicular to the principal goniometer axis and, for zero rotation of the goniometer axis, to the incident beam (in degrees)
(2) Entry in the category `_refln_[]`		
`_refln_frame_id`	Integer number	Integer identifier of the frame on which current reflection was integrated

mined from the orientation matrix of the crystal and the positional angle (or angles) of the goniometer. However, a number of effects may cause a difference between the calculated crystal orientation and the real orientation. These effects include inaccuracy in the orientation matrix, inaccuracy in the positioning of the goniometer or small movements of the crystal during the experiment. It may therefore be necessary to adjust the orientation for each pattern separately. It is important to note that the refinement of the orientation cannot be included in the least-squares refinement together with other parameters. The reason is that a change of orientation results in a change of excitation errors $S_{\mathbf{g}}$, and hence a change in the set of reflections included in the structure matrix $\mathbf{A}$ [equation (3), §2.1]. Hence, the intensities are not smooth functions of the orientation parameters, and least-squares refinement, which is based on an assumption of a smooth gradient, would be unstable. The optimal orientation must be found by a more robust procedure. We use a search for the minimum wR(all) factor as a function of the tilt azimuth and tilt amplitude by means of the downhill simplex algorithm. The details of the procedure are described in paper I, §3.2.

3. Implementation

The option for dynamical refinement has been implemented in the data-processing program *PETS* (Palatinus, 2011) and crystallographic computing system *Jana2006* (Petříček *et al.*, 2014). This section describes the details of the implementation.

3.1. Data processing

The computer program *PETS* is a simple program for processing data from electron diffraction tomography. It allows peak extraction from a series of diffraction patterns, processing raw peak positions and producing a list of peak coordinates in reciprocal space. This list can be used for indexing the diffraction pattern and finding the orientation matrix, *e.g.* with the dedicated graphical interface available in *Jana2006*. With the orientation matrix available, *PETS* can locate and integrate the diffracted intensities. In the standard mode, the reflection intensities are integrated on each frame, but also across the frames, to obtain a total integrated intensity of each reflection. This mode is useful for structure solution and refinement using the kinematical approximation. If, however, the integration option for dynamical refinement is invoked, *PETS* extracts and outputs intensities on each pattern separately. A limit on $|\mathbf{g}|$ and on $S_{\mathbf{g}}^{\rm int}$ is used to decide which reflections should be integrated on a given frame. The limit on $S_{\mathbf{g}}^{\rm int}$ should be set large enough to encompass all potentially interesting reflections. Final data filtering according to the parameters defined in §2.4 is performed in later stages of the procedure. The output from *PETS* is a CIF-like file with most entries encoded as standard CIF entries. However, the entries necessary for the definition of individual patterns are not part of the standard CIF dictionary. These entries are described and defined in Table 1.

3.2. Import of the data to *Jana2006*

The typical procedure for the solution and refinement of an unknown phase is to solve the structure, perform kinematical refinement and then switch to the dynamical refinement. In such a case the structure project is already set up in *Jana2006*. It is only necessary to replace the data set for kinematical refinement by the data set for dynamical refinement using the data import wizard. During the data import, *Jana2006* reads the orientation matrix, information about individual frames (positional angles, precession angle) and the list of reflection intensities. Each entry in the list has a frame number associated with it. It is possible to sequentially read more data sets from different crystals and to combine these data sets in the refinement.

3.3. Setting the data-selection and calculation parameters

Most of the parameters and settings relevant to dynamical refinement are concentrated in the dialog *Electron diffraction* (Fig. 3). The dialog is divided into three sections. The top

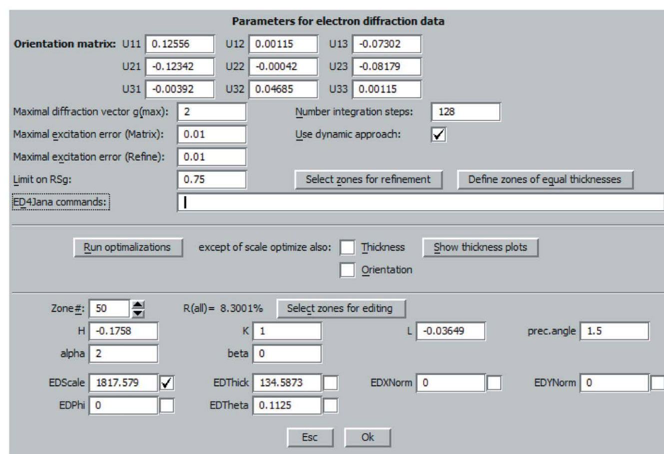

Figure 3
The dialog window 'Electron diffraction' of *Jana2006*, which allows the setting of parameters specific to dynamical refinement of electron-diffraction data.

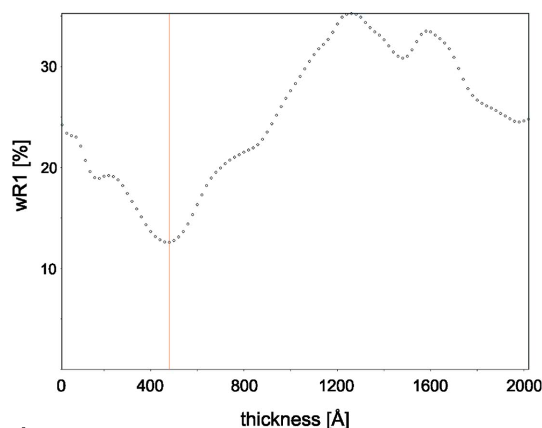

Figure 4
An example of a plot of $wR1$ as a function of thickness for one frame produced by *Jana2006*. The red vertical line shows the thickness with the minimum $wR1$.

section contains the general settings of the refinement, the middle section contains commands for optimization of scale, thickness and orientation of the frames, and the bottom section contains information about individual frames. The general parameters of the refinement are:

(i) Orientation matrix: defines the orientation of the crystal with respect to the microscope coordinate system at zero positional angles.

(ii) Maximal diffraction vector g(max): resolution limit on the reflections entering the structure matrix **A** [equation (3)].

(iii) Maximal excitation error (Matrix): limit on the excitation error of reflections entering the structure matrix **A**.

(iv) Maximal excitation error (Refine): limit on the excitation error of reflections included in the structure refinement. This is the filter on $S_{\mathbf{g}}^{0}$ described in §2.4.

(v) RSg: limit on the parameter $R_{S_{\mathbf{g}}}$ (see §2.4) of reflections included in the structure refinement.

(vi) Number of integration steps: number of steps along the precession circuit for the integration of PED intensities (see §2.2).

Note the principal difference between the parameters labelled 'Maximal excitation error (Matrix)' and 'Maximal excitation error (Refine)'. The former influences the number of beams entering the structure matrix and is purely a parameter of the calculation of dynamical intensities without any relationship to experimentally measured data. The latter is the data-selection filter. It selects a subset from the full list of available reflection intensities, which is then used for the structure refinement. Similarly, the 'Maximal diffraction vector g(max)' is a purely computational parameter and not a data filter, while RSg is a data filter. Obviously, all reflections that pass the data-selection filters must also pass the filters for structure matrix entries. Otherwise their model intensities would not be calculated at all.

3.4. Initial estimation of thickness

Prior to starting the least-squares refinement, initial global estimation of thickness must be performed. This is achieved by calculating the weighted R value on all reflections [wR(all)] for a range of thicknesses between 0 and 2000 Å. Such calculation is performed for each frame. Thickness curves can be plotted for each frame (Fig. 4). They allow an initial assessment of the data quality, and allow exclusion of frames that are unsuitable for refinement in these initial stages. The change of effective thickness with the tilting of the crystal is taken into account internally, and the reported thickness is always related to the true thickness of the slab, not the projected thickness of the tilted slab. If a constant crystal thickness is expected for all frames, the estimated thicknesses may be averaged to obtain a single starting thickness value for the refinement, and only one overall thickness parameter may be refined.

3.5. Least-squares refinement

The structure-refinement procedure is the same as in the case of X-ray diffraction data. The procedures existing in *Jana2006* for full-matrix non-linear least-squares refinement are used. The only point where the present method differs from the standard is the calculation of model intensities $I^{\rm calc}$ and their derivatives with respect to the refined parameters, which are necessary to build the matrix of normal equations for least-squares calculation. Instead of using the relationship $I_{\mathbf{h}} = |F_{\mathbf{h}}|^2$, intensities and their derivatives are calculated using the dynamical-diffraction theory as described in §2.1. The result of the calculation is then used to build the matrix of normal equations, and the refinement proceeds as usual. This approach makes it possible to use seamlessly all the crystallographic tools available in *Jana2006*, like various types of constraints, restraints, reflection selection criteria, automatic restrictions on symmetry *etc.* Technically, the dynamical calculations are performed in a separate executable, which is invoked by *Jana2006* and which returns all necessary quantities. This solution was adopted to allow the use of parallel computing, which is not yet available in *Jana2006*.

The refinement can involve any structural parameter available in *Jana2006*, typically atomic positions, occupancies and displacement parameters. In addition to the structure

parameters, the refinement involves optimization of crystal thickness and also scale parameters of individual frames. These scale parameters represent a significant number of refined parameters, because there are typically several dozens or even over a hundred frames in an EDT data set. However, it appears to be necessary to refine these parameters independently. The reason is that the scale on diffracted intensities does not depend only on the irradiated volume, but also on the irradiated area. This area changes as the crystal is tilted, and the scale thus varies from frame to frame. Moreover, the scale might depend on other quantities which are not easily controllable in the experiment. Refining the scale parameters of each frame separately is a way of avoiding complicated and potentially inaccurate estimation of the scale factor by other means. It must only be ensured that the data-to-parameter ratio remains sufficiently large.

4. Example

The method was tested on a series of samples. A thorough discussion of all aspects of the refinement, optimal values of parameters, improvement obtained with respect to the kinematical refinement *etc.* requires a separate, dedicated publication. Moreover, it is surprisingly difficult to find an example void of any problems and requiring no detailed discussion. In this work we therefore restrict the demonstration only to one illustrative example. The selected compound is a thin nanowire of Ni_2Si (Fig. 5). So far, the structure of Ni_2Si has been obtained only by a powder X-ray diffraction study (Landrum *et al.*, 1998). The precession EDT (PEDT) experiment was performed on a Philips CM120 transmission electron microscope equipped with a Nanomegas Digistar precession device and an upper-mounted CCD camera Olympus Veleta with 14-bit dynamic range. The diffraction data were processed with

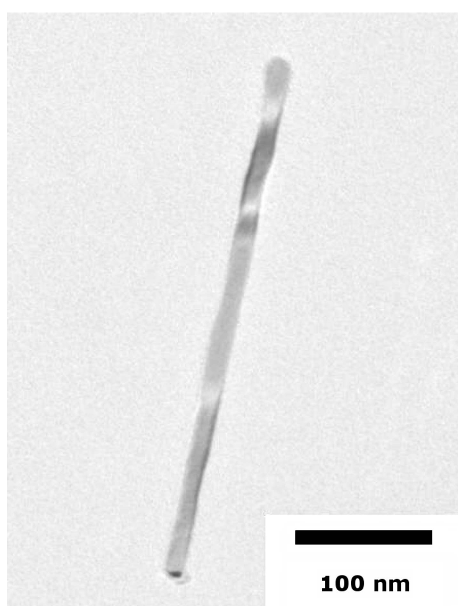

Figure 5
Image of the nanowire of Ni_2Si used to collect data for the structure refinement.

Table 2
Experimental and refinement details of the kinematical and dynamical refinement of an Ni_2Si nanowire.

Space group	*Pnma*
a (Å)	5.041
b (Å)	3.741
c (Å)	7.151
V_{uc} (Å^3)	134.87
Density (g cm^{-3})	7.15
Z	4
λ (Å)	0.0335
Resolution (Å)	0.714
No. of recorded frames	95
Precession angle φ (°)	1.5

	Kinematical	Dynamical
R_{int} (obs/all) (%)	20.35/20.69	
Completeness (%)	93.7	94.6
No. of reflections (obs/all)	169/208	1162/2166
No. of structural parameters	9	9
No. of scale factors	1	95
g_{max} (Å^{-1})		2
S_g^{max} (matrix) (Å^{-1})		0.01
S_g^{max} (refine) (Å^{-1})		0.05
$R_{S_g}^{max}$		0.75
Refined average thickness (nm)		8.6 (1)
R (obs/all) (%)	16.38/18.59	8.82/14.56
wR (obs/all) (%)	19.94/20.03	8.68/9.04
Goodness of fit (obs/all) (%)	11.59/10.43	3.23/2.47

PETS and refined by *Jana2006* using both the standard kinematical approximation and the new dynamical refinement presented in this work. The experimental and refinement details are summarized in Table 2.

Table 3 compares the refined fractional coordinates obtained by kinematical refinement, dynamical refinement and the reference powder X-ray diffraction experiment (Landrum *et al.*, 1998). It is seen that, for most fractional coordinates, the dynamical refinement yields values closer to the X-ray structure, and where the agreement is worse, the difference is small. The maximum distance to the corresponding atomic position in the reference structure decreased from 0.042 Å for kinematical refinement to 0.020 Å for dynamical refinement. Moreover, the the e.s.d.'s of the fractional coordinates from Landrum *et al.* (1998) are on average about twice as large as the e.s.d.'s of the dynamical refinement. Thus, the inaccuracy of the parameters in the reference structure may be significantly contributing to the distances. The results show that the dynamical refinement of a structure obtained from a single nanowire provides results at least comparable, if not superior, to the results of the Rietveld refinement from the bulk powder sample. The improvement over the kinematical refinement is significant despite the fact that the crystal was very thin and the kinematical refinement yielded very good results, if compared with typical kinematical refinements (Kolb *et al.*, 2011).

5. Conclusions and outlook

We have introduced a method for accurate refinement of crystal structures from single-crystal data collected by electron

Table 3
Fractional coordinates for the three independent atoms obtained by kinematical and dynamical refinement and from the reference structure (Landrum *et al.*, 1998).

Distances to the reference structure are also shown. The fractional coordinate y is symmetry restricted to 0.25 for all atoms.

Atom	Coordinate	Kinematical	Dynamical	Reference
Ni1	x	0.0420 (13)	0.0427 (3)	0.0405 (7)
	z	0.7066 (11)	0.7066 (3)	0.7053 (4)
Ni2	x	0.1725 (13)	0.1699 (3)	0.1682 (7)
	z	0.0618 (12)	0.0627 (3)	0.0602 (4)
Si1	x	0.2165 (23)	0.2118 (6)	0.2096 (15)
	z	0.3881 (17)	0.3866 (4)	0.3849 (9)
Distance to the position in the reference structure (Å)				
Ni1		0.012 (8)	0.014 (4)	
Ni2		0.025 (8)	0.020 (4)	
Si1		0.042 (14)	0.016 (8)	

diffraction tomography. The model intensities are calculated using the dynamical-diffraction theory, and thus allow a more accurate and statistically meaningful treatment of the data than the refinements using kinematical approximation. The procedure has been implemented in the computer programs *PETS* and *Jana2006*. The implementation is governed by the principle that the whole method should resemble the standard refinement procedure used in single-crystal X-ray diffraction. This should make the method easily accessible to all crystallographers skilled in standard structure analysis. The method was tested on a number of crystal structures of variable complexity, for which the reference structure obtained by X-ray diffraction was available. These tests show that the method is usable in practice and they also give insight into the optimal setting of the parameters of the method. Because of the large amount of information that needs to be presented, we limited the presentation in this paper to only one illustrative example. A full discussion of the test cases will be presented in a separate article.

APPENDIX *A*
Analytical expressions for cumulative distribution functions of thickness for some idealized crystal shapes

Assuming that the thickness probability distribution function $f(t)$ is known, the diffracted intensity can be calculated within the approximation of incoherent superposition as

$$I_{\mathbf{h}} = \int_{t_{\min}}^{t_{\max}} I_{\mathbf{h}}(t) f(t)\,\mathrm{d}t. \qquad (10)$$

During numerical evaluation of this expression, the intensity is evaluated as a function of thickness in a set of n discrete intervals between $t_{\min}$ and $t_{\max}$ in steps of Δt. The total intensity must be approximated by a discrete summation:

$$I_{\mathbf{h}} \simeq \sum_{i=1}^{n} \left[I_{\mathbf{h}}(t_i) \int_{t_i-\Delta t/2}^{t_i+\Delta t/2} f(t)\,\mathrm{d}t \right] = \sum_{i=1}^{n} I_{\mathbf{h}}(t_i)\left[F(t_i+\Delta t/2) - F(t_i-\Delta t/2)\right]. \qquad (11)$$

In this equation $F(t)$ represents the cumulative distribution function corresponding to the probability distribution function $f(t)$, and the special form of the summation terms at t_1 and t_n was omitted for simplicity.

In the following sections we derive the analytical expressions for the cumulative distribution functions for thickesses of four model crystal shapes: wedge, cylinder, ribbon with lens-like intersection and a convex lens.

Before doing so we define the conventions and notation used throughout this appendix: (i) the beam is assumed to be coming to the crystal vertically, *i.e.* along the z axis of the coordinate system; (ii) t, thickness measured along the incident beam direction; (iii) D, the maximum lateral length of the crystal; (iv) t_m, the maximum thickness of the crystal; (v) f, 'flatness parameter', $f = t_m/D$; (vi) τ, reduced thickness, $\tau = t/t_m$; (vii) x, lateral distance from the origin of the coordinate system.

A1. Wedge

A wedge-shaped crystal has a linear dependence of the thickness on the lateral coordinate x. $F(t)$ is thus proportional to t (Fig. 6*a*), and because for $t = t_m$ $F(t)$ must be equal to 1, we get a very simple result in terms of the reduced thickness τ:

$$F(\tau) = \tau. \qquad (12)$$

A2. Cylinder

A long cylinder is a model for a nanowire or needle-shaped crystal. For simplicity we will consider only a cylinder lying perpendicular to the incoming beam. The problem then reduces to a two-dimensional problem of determining the $F(t)$ of a circle. The maximum thickness in the cylinder is equal to its diameter. $F(t)$ can be determined from the following consideration: a certain thickness t is encountered in the circle only twice, at positions $\pm x$, where x is given by

$$x = \left[\left(\frac{D}{2}\right)^2 - \left(\frac{t}{2}\right)^2\right]^{1/2}. \qquad (13)$$

The value of $F(t)$, *i.e.* the probability that a vertical beam hitting the crystal encounters a smaller thickness than t, is given by the ratio $(D-2x)/D = 1 - 2x/D$ (Fig. 6*b*). Recalling that $t_m = D$, substituting equation (13) for x and simplifying the expression, we obtain

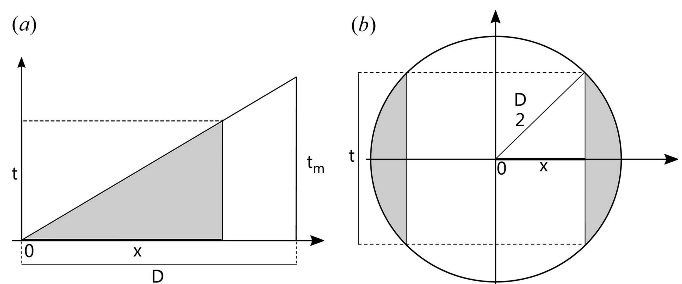

Figure 6
Cross section of a wedge-shaped crystal (*a*) and a cylindrical crystal (*b*). Shaded areas highlight the parts of the crystals thinner than t.

$$F(t) = 1 - \left[1 - \left(\frac{t}{t_m}\right)^2\right]^{1/2}, \quad (14)$$

or, in terms of the reduced thickness,

$$F(\tau) = 1 - (1 - \tau^2)^{1/2}. \quad (15)$$

A3. Ribbon with lens-shaped cross section

As in the case of a cylinder, the problem in this case can be reduced to two dimensions. A lens in two dimensions can be described as an intersection of two discs of equal radius displaced with respect to each other in the vertical direction (Fig. 7*a*). The general expression for $F(t)$ remains the same as for a cylinder: $F(t) = 1 - 2x/D$, where x is the lateral distance from the centre of the lens, at which the lens has thickness t (Fig. 7*a*). The expression for x as a function of t is

$$x = \left\{\left[\frac{(D/2)^2 + (t_m/2)^2}{t_m}\right]^2 - \left[\frac{t}{2} + \frac{(D/2)^2 - (t_m/2)^2}{t_m}\right]^2\right\}^{1/2}. \quad (16)$$

This expression simplifies greatly if we use the flatness parameter f and reduced thickness τ:

$$x = \frac{D}{2}\left[1 - \tau^2 f^2 - \tau(1 - f^2)\right]^{1/2}. \quad (17)$$

The cumulative distribution function then becomes

$$F(\tau) = 1 - \left[1 - \tau^2 f^2 - \tau(1 - f^2)\right]^{1/2}. \quad (18)$$

The formula reduces to that for the cylinder for $f = 1$.

A4. Convex lens

A standard convex lens is generated by the rotation of the two-dimensional lens from the previous case around the vertical axis. Following the same consideration as above, we conclude that $F(t)$ in this case is given by the ratio of the area of the lens with thickness smaller than t to the total area (Fig. 7). Let x be the lateral distance from the centre of the lens at which the lens has thickness t. Then

$$F(\tau) = \frac{\pi\left[(D/2)^2 - x^2\right]}{\pi(D/2)^2} = 1 - \left(\frac{2x}{D}\right)^2. \quad (19)$$

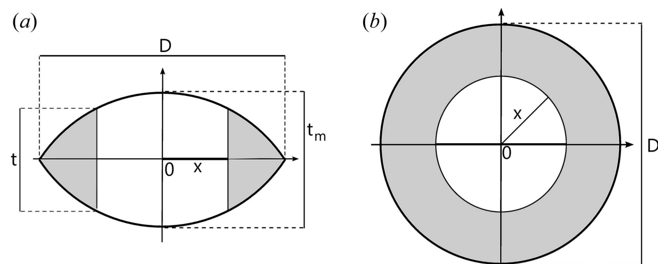

Figure 7
(*a*) Lens in two dimensions formed by the intersection of two discs with the same radius displaced with respect to each other in the vertical direction. (*b*) A top view of a circular convex lens with shaded area representing the part of the lens with thickness smaller than t.

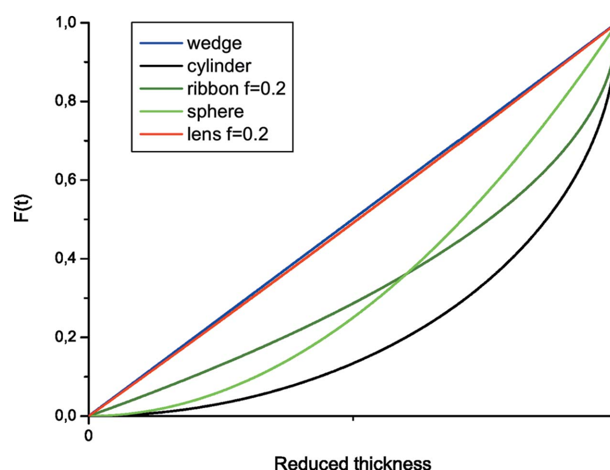

Figure 8
Cumulative density function as a function of the reduced thickness plotted for a wedge, cylinder, ribbon (two-dimensional lens), sphere and a convex lens.

Expression for x is given by equation (17). Plugging equation (17) into the above expression we obtain the result

$$F(\tau) = \tau^2 f^2 + \tau(1 - f^2). \quad (20)$$

Setting $f = 1$ we obtain an especially simple expression for a sphere: $F(\tau) = \tau^2$. For a very flat lens ($f \to 0$) $F(\tau) \to \tau$ and has thus the same form as $F(\tau)$ of a wedge.

Cumulative distribution functions of other shapes can be derived analogically to the examples above. Plots of cumulative probability functions of selected shapes are shown in Fig. 8. It should be noted that using equation (11) for calculating the intensities does not make the calculation much more time consuming. This is because only one matrix diagonalization is required for calculating intensities at several thicknesses. Calculating intensities at 20 different thickness values instead of one increases the computing time by approximately 40%.

Acknowledgements

This work was funded by the grant agency of the Czech Republic (grant No. 13-25747S). LP acknowledges the support of his research through a J. E. Purkyně Fellowship awarded by the Academy of Sciences of the Czech Republic.

References

Aa, N. P. van der, ter Morsche, H. G. & Mattheij, R. R. M. (2007). *Electron. J. Linear Algebra*, **16**, 200–314.
Berg, B. S., Hansen, V., Midgley, P. A. & Gjønnes, J. (1998). *Ultramicroscopy*, **74**, 147–157.
Bird, D. M. & King, Q. A. (1990). *Acta Cryst.* A**46**, 202–208.
Cowley, J. M. (1992). *Electron Diffraction Techniques*, Vols 1 and 2. Oxford University Press.
Dorset, D. L. (1995). *Structural Electron Crystallography*. New York: Plenum Press.
Dudka, A. P., Avilov, A. S. & Lepeshov, G. G. (2008). *Crystallogr. Rep.* **53**, 530–536.
Hirsch, P., Howie, A., Nicholson, R., Pashley, D. & Whelan, M. (1977). *Electron Microscopy of Thin Crystals*. Florida: Robert E. Krieger.
Jansen, J., Tang, D., Zandbergen, H. W. & Schenk, H. (1998). *Acta Cryst.* A**54**, 91–101.

Kolb, U., Gorelik, T., Kuebel, C., Otten, M. T. & Hubert, D. (2007). *Ultramicroscopy*, **107**, 507–513.
Kolb, U., Gorelik, T. & Otten, M. T. (2008). *Ultramicroscopy*, **108**, 763–772.
Kolb, U., Mugnaioli, E. & Gorelik, T. (2011). *Cryst. Res. Technol.* **46**, 542–554.
Landrum, G. A., Hoffmann, R., Evers, J. & Baysen, J. (1998). *Inorg. Chem.* **37**, 5754–5763.
Metherel, A. (1975). In *Electron Microscopy in Materials Science II*, edited by U. Valdré & E. Ruedl, pp. 401–552. Brussels: CEC.
Mugnaioli, E., Gorelik, T. & Kolb, U. (2009). *Ultramicroscopy*, **109**, 758–765.
Oleynikov, P. (2011). *Cryst. Res. Technol.* **46**, 569–579.
Own, C. S., Marks, L. D. & Sinkler, W. (2006). *Acta Cryst.* A**62**, 434–443.
Palatinus, L. (2011). *PETS – program for analysis of electron diffraction data.* Prague: Institute of Physics of the AS CR.
Palatinus, L., Jacob, D., Cuvillier, P., Klementová, M., Sinkler, W. & Marks, L. D. (2013). *Acta Cryst.* A**69**, 171–188.
Palatinus, L., Klementova, M., Drinek, V., Jarosova, M. & Petříček, V. (2011). *Inorg. Chem.* **50**, 3743–3751.
Petříček, V., Dušek, M. & Palatinus, L. (2014). *Z. Kristallogr.* **229**, 345–352.
Spence, J. & Zuo, J. M. (1992). *Electron Microdiffraction.* New York: Plenum Press.
Vainshtein, B. K. (1964). *Electron Diffraction Structure Analysis.* Oxford: Pergamon Press.
Vincent, R. & Midgley, P. A. (1994). *Ultramicroscopy*, **53**, 271–282.
Wan, W., Sun, J., Su, J., Hovmöller, S. & Zou, X. (2013). *J. Appl. Cryst.* **46**, 1863–1873.
Weickenmeier, A. & Kohl, H. (1991). *Acta Cryst.* A**47**, 590–597.